

Article

Interval Type-2 Fuzzy-Logic-Based Constant Switching Frequency Control of a Sliding-Mode-Controlled DC–DC Boost Converter

Güven Balta ¹, Necmi Altin ² and Adel Nasiri ^{3,*}

¹ Electrical-Electronics Engineering Department, Faculty of Engineering and Architecture, Erzurum Technical University, Erzurum 25050, Turkey

² Electrical-Electronics Engineering Department, Faculty of Technology, Gazi University, Ankara 06560, Turkey

³ Electrical Engineering Department, College of Engineering and Computing, University of South Carolina (USC), Columbia, SC 29208, USA

* Correspondence: nasiri@sc.edu; Tel.: +1-803-576-7796

Abstract: The inherent unlimited high switching frequency of the sliding mode controller (SMC) is limited by practical constraints of the hysteresis modulation (HM) technique. The inductor current and output voltage of a converter can be regulated using a combination of HM-SMC. However, HM-SMC results in a variable switching frequency operation, which is not preferred due to Electromagnetic Interference (EMI) issues. In this paper, an interval fuzzy controller is designed and developed as a solution to enable HM-SMC. In addition, a robust sliding surface is proposed, which provides an improved dynamic response. The two proposed controllers' compatibility with one another has been tested via experiments such as a step change in input voltage, load resistance variation, and finally, a step change in output voltage reference value. The test results validate that while the interval type-2 fuzzy maintains a constant switching frequency with acceptable dynamic responses, it successfully regulates the state variables of the system. A comparison of the performance of the proposed control method with existing techniques in the literature is presented.

Keywords: constant switching frequency; DC–DC boost converter; sliding mode control; type-2 fuzzy logic controller



Citation: Balta, G.; Altin, N.; Nasiri, A. Interval Type-2 Fuzzy-Logic-Based Constant Switching Frequency Control of a Sliding-Mode-Controlled DC–DC Boost Converter. *Appl. Sci.* **2023**, *13*, 3239. <https://doi.org/10.3390/app13053239>

Academic Editor: Luis Hernández-Callejo

Received: 30 January 2023
Revised: 22 February 2023
Accepted: 28 February 2023
Published: 3 March 2023



Copyright: © 2023 by the authors. Licensee MDPI, Basel, Switzerland. This article is an open access article distributed under the terms and conditions of the Creative Commons Attribution (CC BY) license (<https://creativecommons.org/licenses/by/4.0/>).

1. Introduction

Reduction in operating switching frequency is an important requirement when implementing sliding mode control (SMC) for power electronic converters. An ideal SMC suggests that the switching frequency is high enough to consider the state variables are constant during a switching period and that the system's trajectories slide along a switching surface in such a way that the required dynamics are realized [1]. On the other hand, such a high switching frequency in a closed-loop control system causes substantial difficulty in calculating state variables known as chattering. In addition, it is also not feasible for practical power converters to operate at extremely high switching frequencies due to limitations of semiconductor power switches and added power loss. Chattering also causes poor control precision and high heat in power converters [2,3]. In addition, the switching frequency has a considerable influence on the structural design of the converters since it directly impacts the size of inductors and capacitors as well as the switches themselves [1,4]. Therefore, it is preferable to have an optimized and stable switching frequency. To nullify major drawbacks associated with the natural operation of the SMC and also to achieve a switching frequency, HM has been utilized by the scientific community since it offers some outstanding features such as simple implementation, generation of a switching signal without the need for a trigger signal, and no need for including a saturation function. In this method, the state trajectory is forced to move inside the region enclosed by constant or adaptive symmetric band values, which leads to reduced chattering and a narrow

range of the switching frequency [1,2,5]. A satisfactory output voltage regulation with a smooth inductor current regulation have been achieved successfully [1,4,5]. Although it is an extremely effective technique, it unavoidably results in a time-varying switching frequency. High and time-varying switching frequencies result in steady-state errors, high switching losses, challenging output filter designs [5], EMI noises [3], and a reduction in the converters' capacity to regulate the voltage and current. Even though controlling the switching frequency is essential, it has not received as much attention in past research work. As a result, there are few similar investigations in the body of existing literature.

As previously mentioned, there are a number of HM-based SMC studies in the literature, and research on this subject is accelerating at a high rate to provide appropriate transient and steady-state performance. Unfortunately, most HM-SMC investigations in the literature have concentrated solely on output voltage control [6–9] or combination with inductor current control [10–14], disregarding variable switching frequency. To precisely address this need, the study in [4] presents a novel switching frequency controller based on the assumption of piecewise linear behavior of the sliding surface. The study formulates a new closed-loop control that measures the switching period, uses a frequency controller loop (FCL) to update the hysteresis band value, and drives the measured switching period to converge to a predetermined reference value. The outcomes show that both the switching frequency and state variables are effectively maintained at the reference levels, even during transitions. Because of its effectiveness, the FCL strategy has also been used with different sliding manifolds, such as fast terminal sliding surfaces [15]. Despite such improved outcomes of FCL, the technique necessitates a calibration for the other system variables as well as the switching frequency, adding computing complexity. The switching frequency calibration also gives a coefficient that has a considerable effect on the switching frequency, as shown in [15], as well as other system state variables, notably on the output voltage. Thus, the control system contains far too many coefficients as a result of the FCL and the designed sliding surface, making it very challenging to adjust the coefficients. The fine-tuning of the coefficients becomes extremely difficult because it must be performed with great care and precision while taking into account all state variables.

In order to completely eliminate the aforementioned disadvantages, namely reducing the mathematical complexity in the system, preventing the state variables and switching frequency from being affected by the coefficients of the switching frequency controller, and minimizing the amount of coefficient to be tuned, in this study, a type-2 fuzzy logic control is proposed to keep the switching frequency at a desired value for the SMC-controlled DC–DC converter. In addition, a robust sliding surface has been proposed in this study to eliminate the steady-state error and to achieve a fast transient response. Since it is an essential element for a variety of applications, for example, fuel cells, electric drives, renewable energy systems, and welding machines [8,16,17], a DC–DC boost converter is employed to illustrate the effectiveness of the formulated control structures. Despite its widespread application, the converter has several drawbacks. It has a time-varying, non-smooth, and inherent nonlinear dynamic [8,15]. It is also extremely vulnerable to recurring input voltage variations as a result of unstable supply and unforeseen load disturbances [15,16]. All of these unfavorable circumstances lower the converter's performance. This also means that the systems in which the converter is employed will also suffer. Due to the fact that any increase in the converter's performance would benefit all of the involved systems, an improvement in the converter's performance becomes even more important. Apart from this, the Boost converter has a non-minimum phase structure, i.e., the control input exists in both voltage and current equations [18]. That is why controlling it is more difficult than minimum phase power converters such as buck, half-bridge, and voltage source inverters. As the control methods described in this research produce more efficient outcomes, it is ensured that they can be effortlessly used for minimum-phase power converters.

When compared to the previous studies, this study introduces four advanced innovations, listed as follows:

- (1) In this study, a type-2 fuzzy logic controller is employed for switching frequency control, which has never been formulated previously.
- (2) By providing both open-loop and closed-loop evaluation of the switching frequency, it is described how the system characteristics impact the switching frequency.
- (3) The effectiveness of the suggested surface for system dynamics has been demonstrated by comparing it to various sliding surfaces in the literature.
- (4) The results obtained by the proposed controllers and other controllers in the literature are compared, and the efficacy of the proposed methods are validated.

The rest of this paper is organized as follows: The mathematical model of the boost converter is obtained in Section 2. An overview of the sliding-mode controller is given in Section 3. In Section 4, the factors that affect switching frequency are discussed in detail, along with the interval type-2 fuzzy system (IT2FS) that is suggested for the switching frequency control. The design and implementation of the proposed strategies are introduced in Section 5. The determination of the parameters of the proposed SMC method is also covered in this section. Finally, the conclusions are drawn in Section 6.

2. Mathematical Analysis of Boost Converter

Figure 1 depicts a common DC–DC boost converter diagram. It consists of an inductor (L), a filter capacitor (C), a semiconductor switch (S_w), and a diode (D). The input voltage, load resistance, and output current are denoted with E , R , and I_o , respectively. During the converter modeling, the converter parameters and power switch are assumed to be ideal. It is also assumed that the converter is operating in continuous conduction mode. According to the ON and OFF conditions of the switch, the boost converter has two separate functioning modes. Based on two different modes, the average state space model of the converter can be constructed as [8]:

$$\begin{aligned} \frac{dI_L}{dt} &= \frac{E}{L} - \frac{(1-u)V_0}{L} \\ \frac{dV_0}{dt} &= \frac{(1-u)I_L}{C} - \frac{V_0}{RC} \end{aligned} \tag{1}$$

where I_L is the inductor current, V_0 is the output voltage, u is the control signal, which takes '0' for the OFF state and '1' for the ON state of the switch.

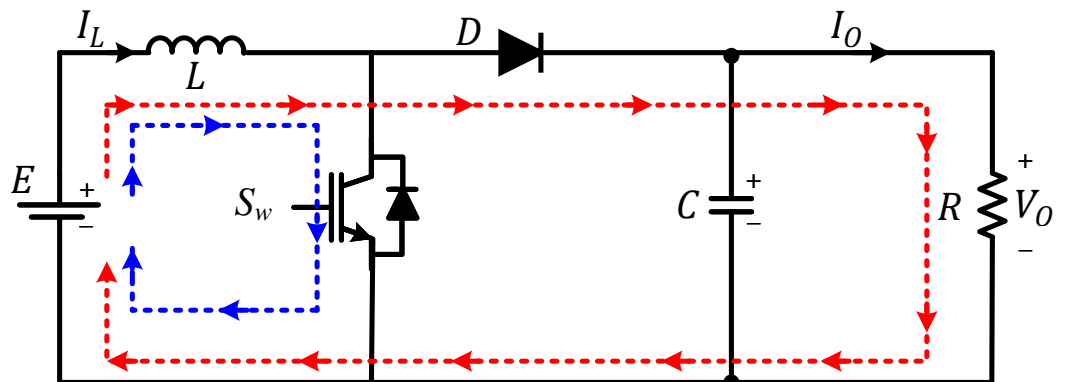


Figure 1. Boost converter (blue line: the switch is ON, red line: the switch is OFF).

3. Design of Sliding Mode Controller

The SMC is designed in two steps. One of the two steps is determining a suitable sliding manifold [7]. The designed sliding surface is given below [1]

$$S = \lambda x_1 + \beta \int_0^t x_1(t)dt - \gamma I_L \tag{2}$$

where λ, β, γ are the positive parameters, x_1 is the output voltage error, which is defined as $x_1 = V_{ref} - V_0$, and V_{ref} is the reference value of output voltage.

This converter exhibits non-minimum phase characteristics, as seen by the space-state equations in (1). In a more intelligible expression, the control signal is linked to the inductor current as well as the output voltage. This characteristic of the converter precludes direct voltage control [1,18,19]. To address this issue, the inductor variable must be located within the specified surface. The surfaces chosen for non-minimum phase converters in HM-SMC investigations are commonly classified into two major classes in the literature: Firstly, surfaces that depend just on inductor current error [1,11,18,20], and secondly, surfaces that depend on both inductor current error and output voltage error [10,12–14,17,19]. Both categories of surface topologies have their own share of advantages and disadvantages. In the surface utilized in this study, there is no extra value specified for the reference value of the inductance current, and it is generated by using the output voltage error, which makes it the best option.

For the second stage of SMC design, which is the determination of the control law, the following equation is provided from the study in [8].

$$u = \begin{cases} 0 & \text{when } S < -\Delta \\ 1 & \text{when } S > \Delta \end{cases} \tag{3}$$

where Δ is a hysteresis bandwidth. The expression formulated in (3) is derived from the formulation $u = (1 + \text{sign}(S))/2$ because, as highlighted in the introduction section, the formula in (3) enables the practical application and eliminates several additional issues. By the way, it should be noticed that, in some studies, a PWM-based SMC has taken the place of the HM-SMC [3,21,22]. However, the control becomes sensitive to the parameters. In this case, SMC robustness should be re-established by introducing additional terms to compensate for parameter dependence [5]. In addition, with this approach, the control signal is created by comparing it with a trigger signal rather than going directly to the switch. All of these disadvantages result in more complicated control structures.

The stability of sliding mode control is assured if the following criterion is met.

$$S \frac{dS}{dt} < 0 \tag{4}$$

where $\frac{dS}{dt} = \lambda \left(\frac{V_0}{RC} - \frac{(1-u)I_L}{C} \right) + \beta x_1 - \gamma \left(\frac{E}{L} - \frac{(1-u)V_0}{L} \right)$.

Existence conditions, such as the hitting condition mentioned in (3), must be observed for the stable functioning of SMC. With the help of the conditions given in (3) and (4), one can generate the existence conditions shown below [3].

When $S < 0 \Rightarrow u = 0$, then the following inequality can be written for $\dot{S} > 0$

$$\lambda \left(\frac{V_0}{RC} - \frac{I_L}{C} \right) + \beta x_1 - \gamma \left(\frac{E}{L} - \frac{V_0}{L} \right) > 0 \tag{5}$$

When $S > 0 \Rightarrow u = 1$, then the following inequality can be written for $\dot{S} < 0$

$$\lambda \left(\frac{V_0}{RC} \right) + \beta x_1 - \gamma \left(\frac{E}{L} \right) < 0 \tag{6}$$

The coefficients λ, β and γ should be selected to satisfy (5) and (6).

The equivalent control [1,4,8], represented by u_{eq} , is obtained by applying the invariance criterion provided by the following equation.

$$\begin{aligned} \frac{dS}{dt} \Big|_{S=0} &= 0 \\ u &= u_{eq} \\ u_{eq} &= 1 - \frac{-\frac{\lambda V_0}{RC} - \beta x_1 + \frac{\gamma E}{L}}{-\frac{\lambda I_L}{C} + \frac{\gamma V_0}{L}} \end{aligned} \tag{7}$$

The equivalent control ideally keeps the system sliding on S . The sliding movement on the switching surface $S = 0$ is guaranteed when

$$0 < \frac{-\frac{\lambda V_0}{RC} - \beta x_1 + \frac{\gamma E}{L}}{-\frac{\lambda I_L}{C} + \frac{\gamma V_0}{L}} < 1 \tag{8}$$

4. Interval Type-2 Fuzzy Logic Controller for Constant Switching Frequency

Any acceptable constant or flexible value can be used to set the hysteresis bandwidth. The switching frequency should be considered when choosing the hysteresis band value since there is a strong association between them. To figure out the relationship between the switching frequency (f_s) and the hysteresis bandwidth (Δ), Figure 2 can be utilized.

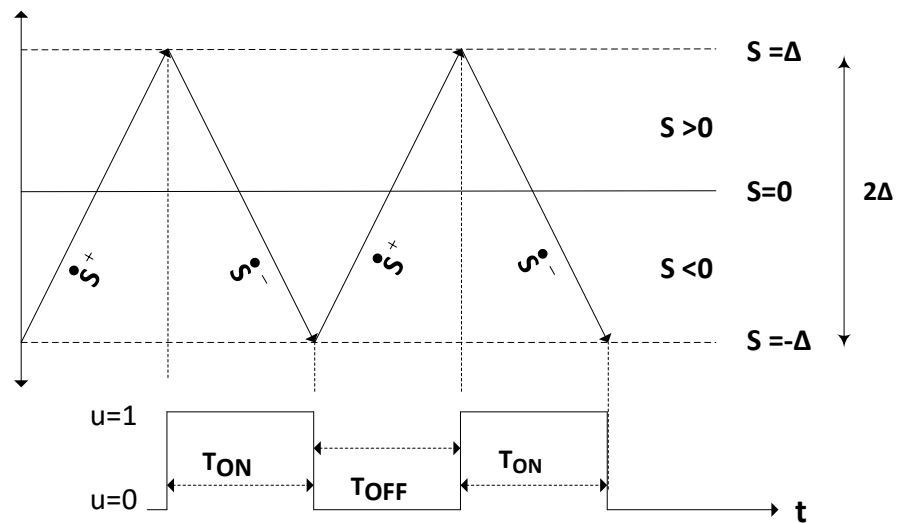


Figure 2. Hysteresis-modulated sliding function.

From the figure, it is required to calculate the derivative of S in order to find the relationship between f_s and Δ . Note that \dot{S}^+ and \dot{S}^- are considered the positive slope and negative slope of the time derivatives of the proposed sliding surface. According to the geometry of Figure 2 and with the help of (2), (5), and (6), the ON and OFF periods of the switch can be expressed as below by assuming that the error variable x_1 is negligible and the desired inductor current is $I_{Ldesired} = \frac{(V_{ref})^2}{RE}$ in the steady state.

$$T_{on} = \frac{-2\Delta}{\dot{S}^-} = \frac{-2\Delta}{\lambda \frac{V_0}{RC} - \gamma \frac{E}{L}} \tag{9}$$

$$T_{off} = \frac{2\Delta}{\dot{S}^+} = \frac{2\Delta}{\lambda \left(\frac{V_0}{RC} - \frac{V_{ref}^2}{REC} \right) - \gamma \left(\frac{E}{L} - \frac{V_0}{L} \right)} \tag{10}$$

With the help of (9) and (10), the expression for the switching frequency can be obtained as

$$f_s = \frac{1}{T_{on} + T_{off}} = \frac{1}{2\Delta \left(\frac{1}{a_1} - \frac{1}{a_2} \right)} \tag{11}$$

where $a_1 = \lambda \left(\frac{V_0}{RC} - \frac{V_{ref}^2}{REC} \right) - \gamma \left(\frac{E-V_0}{L} \right)$ and $a_2 = \lambda \frac{V_0}{RC} - \gamma \frac{E}{L}$.

By choosing an optimal hysteresis bandwidth, one can obtain a desirable switching frequency based on (11). However, this method raises a concern that the switching frequency varies over time as it depends on the parameters of the circuit and also coefficients of the designed surface. This is not desirable, as discussed in the previous section. To remove all

of the problems caused by a time-varying switching frequency and to prevent running the converter at a different switching frequency than that desired, a basic controller should be employed. With the hypothesis of piecewise linear behavior of the sliding function [4,15], the time-varying switching frequency issue can be resolved. Unfortunately, as it was noted, this strategy results in an excessive amount of mathematical complexity. For this reason, type-2 fuzzy logic control is proposed in this study.

Block diagrams of a type-1 fuzzy logic system (T1FS) and a type-2 fuzzy logic system (T2FS) are presented in Figure 3. Both systems operate on the same fundamental principle. Nevertheless, there are some significant distinctions between them. While both T1FS and T2FS have the fuzzification, fuzzy inference engine, knowledge base, and defuzzification, T2FS also has a type-reducer stage that sits between the inference engine and the defuzzifier, as demonstrated in Figure 3. Another difference is that the membership functions of the T1FS are certain, whereas T2FS employs type-2 fuzzy sets, which are described by fuzzy membership functions. By doing so, T2FS are able to simulate and govern measurement uncertainty (converter structure, sensors) as well as any rule uncertainty, resulting in more satisfied dynamic responses [23,24]. In contrast to T1FS, several investigations have also supported this circumstance, namely the robustness of T2FS [23–25].

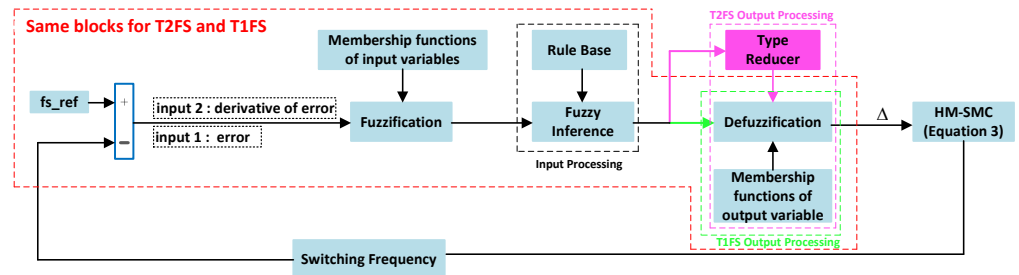


Figure 3. T2FS and T1FS block diagram.

One of the most significant steps in the T2FS design is defining the input and output variables, as well as the controller’s membership functions. Because the switching frequency of the converter is controlled, the input variables of the proposed IT2FS are the switching frequency error (e) and the change in switching frequency error (ce). Figure 4 depicts the five triangle membership functions for the IT2FS input variables. The linguistic variables ‘positive big (PB)’, ‘positive small (PS)’, ‘zero (ZE)’, ‘negative small (NS)’, ‘negative big (NB)’ for two input variables are used to express the fuzzy variables.

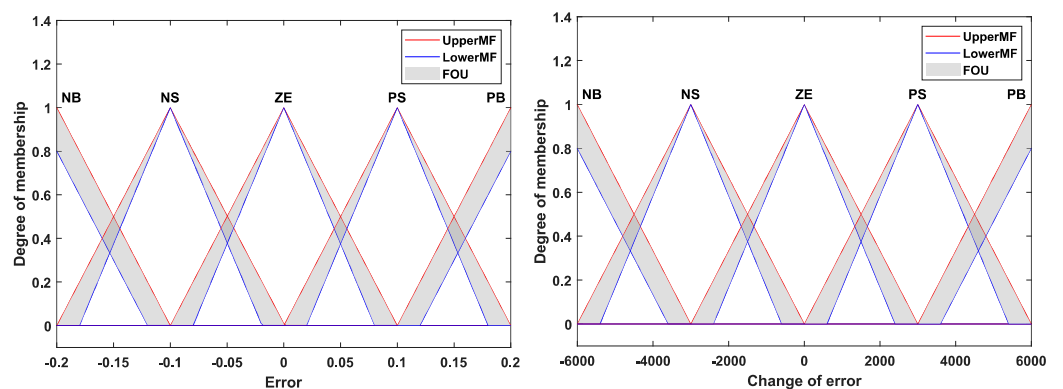


Figure 4. IT2FS membership functions for input variables.

The hysteresis band (Δ) is the output variable of the IT2FS. Five triangle membership functions, which are expressed by the linguistic variables ‘negative big (NB)’, ‘negative small (NS)’, ‘zero (ZE)’, ‘positive small (PS)’, and ‘positive big (PB)’, are determined for the output variable of the IT2FS, as seen in Figure 5. The rules are developed using knowledge

of the system’s functioning in accordance with variations in error and changes in error inputs in order to provide a fast transient response. The rule base of the IT2FS for the output variable ‘hysteresis band value’ is seen in Table 1.

Table 1. Rules of IT2FS.

| Change in Error | Error | | | | |
|-----------------|-------|----|----|----|----|
| | NB | NS | ZE | PS | PB |
| NB | PB | PB | PS | ZE | NS |
| NS | PB | PS | PS | NS | NS |
| ZE | PS | PS | ZE | NS | NS |
| PS | PS | PS | NS | NS | NB |
| PB | PS | ZE | NS | NB | NB |

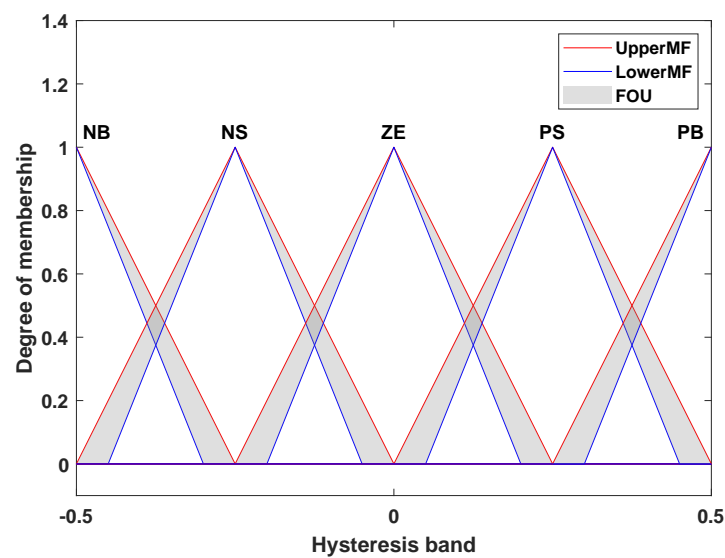


Figure 5. IT2FS membership functions for the output variable.

5. Simulation Results

In this section, several considerations are reviewed to assess the feasibility of the proposed SMC and IT2FS in a DC–DC boost converter. The block diagram of the converter with the proposed methods is depicted in Figure 6. To begin, the DC–DC boost converter is developed in the MATLAB/Simulink environment using components from the Simulink library rather than numerical dynamic equations in (1) to precisely reflect its nature. The sampling time for simulations is defined as 2 μs. The parameters of the considered converter are given in Table 2. Some of these parameters are taken from the study in [1].

Table 2. Boost converter specifications.

| Description | Parameter | Value |
|-------------------------------|--------------|---------|
| Input voltage | E | 12 V |
| Filter capacitor | C | 132 μF |
| Inductor | L | 20 μH |
| Load resistance | R | 20 Ω |
| Output voltage reference | V_{ref} | 48 V |
| Switching frequency reference | f_{s_ref} | 100 kHz |

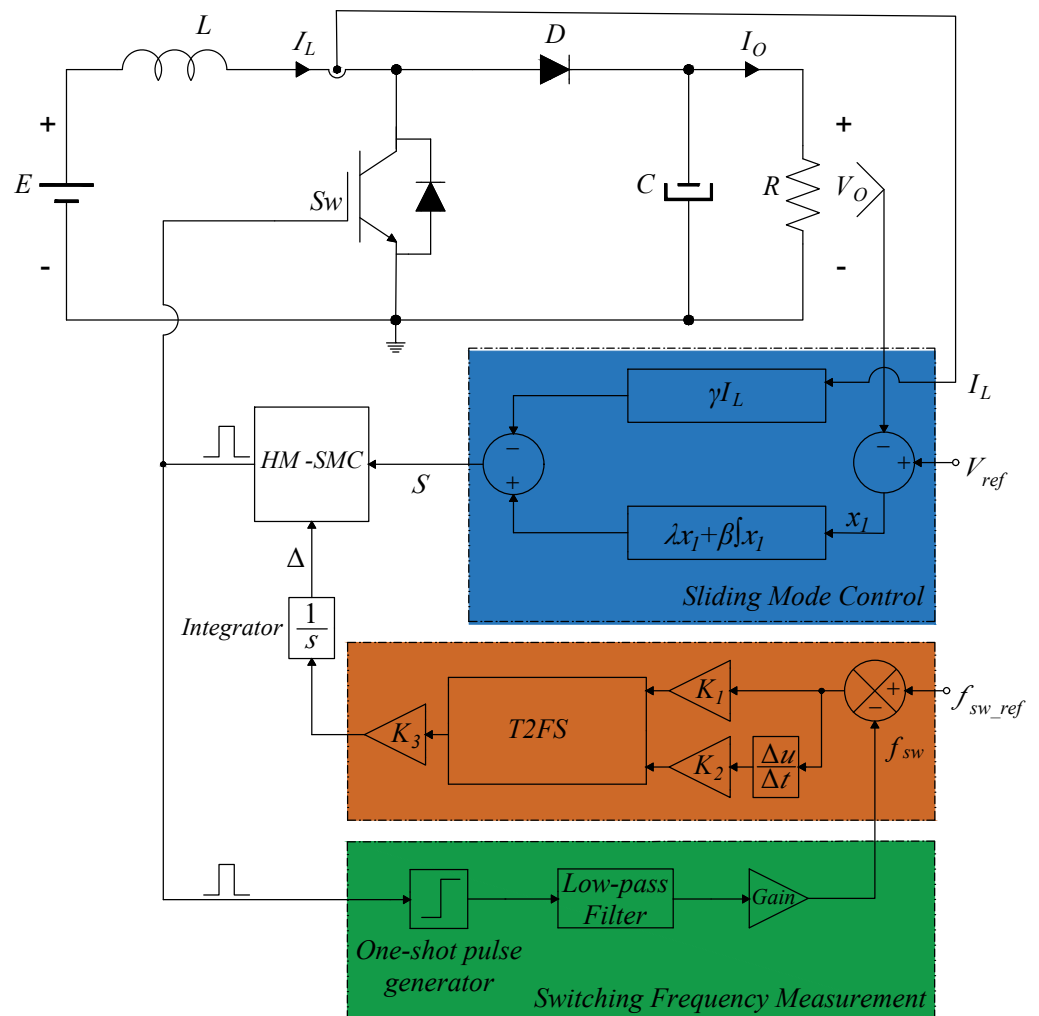


Figure 6. Block diagram of the system.

5.1. Selection of Proposed Voltage Control Coefficients

To make the selection of surface parameters more reasonable, we provide an illustration that shows how the output voltage error and inductor current is impacted by the selection of control parameters. It needs to be acknowledged that there is not yet a quantitative method in the literature for determining the ideal value of the controller coefficients. As a result, a few trial-and-error stages are needed to identify the ideal values of the coefficients for an acceptable performance of state variables. For this reason, the gamma coefficient (γ) is selected, and its effect on both the output voltage and inductor current is explored. The γ parameter is changed with the values of 5, 10, and 25, and the results obtained are plotted in Figure 7. Obviously, as the value of γ is increased, the output voltage converges to its reference value in a shorter time, which is a desirable dynamic response. On the other hand, a higher coefficient value creates a greater ripple in the inductor current, as seen in the same figure, because the switching frequency depends on the coefficients of the surface used, as shown in (11). When these parameters change, the switching frequency also changes, which triggers ripples in the inductor current. Hence, the control coefficients should be chosen with care in order to maintain a balance between the output voltage and inductor current. Taking into consideration the mentioned requirements, the coefficients of the surface proposed in the study are established as $\lambda = 10, \beta = 2000, \gamma = 10$.

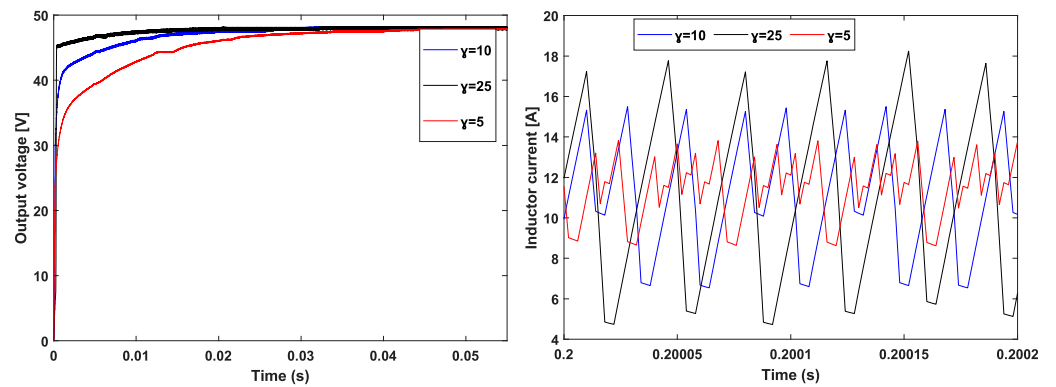


Figure 7. The effect of γ on state variables.

5.2. Comparison with Some Other Sliding Surfaces

A comparison with various sliding surfaces reported for non-minimum phase systems is performed to further confirm the performance of the proposed methodology. The study in [17] suggests the following surface of combinations of state variables with no coefficients.

$$S_1 = I_{Lref}V_0 - V_{ref}I_L \tag{12}$$

Another surface depicted in the literature [19] is given in (13).

$$S_2 = \lambda_1(V_{ref} - V_0) + \gamma_1(I_{ref} - I_L) \tag{13}$$

In contrast to the surfaces suggested in this study, the reference value of the inductor current (I_{Lref}) in these two surfaces cannot be generated automatically; it must be input manually. This has negative effects on the system, which is portrayed in Figures 8 and 9.

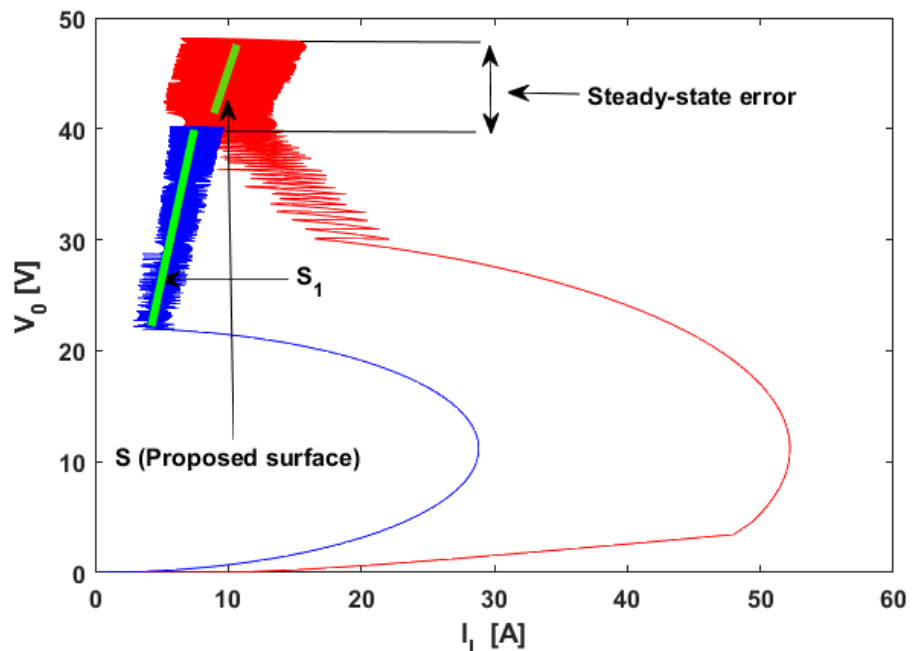


Figure 8. The motion of state variables on the proposed surface and S_1 .

Figure 8 makes it clear that the proposed sliding surface has a better effect on the system dynamics than S_1 . During sliding motions on the surfaces, chattering occurs in the state variables for both S and S_1 . On the other hand, the dynamics of the system with S_1 exhibit very high steady-state errors, such as a 20% inaccuracy in the output voltage. A similar comparison between S and S_2 reveals that S provides better dynamic responses,

as seen in Figure 9. To minimize the steady-state error in the system throughout the simulation of S_2 , the values of $\lambda_1 = 500$ and $\gamma_1 = 1000$ are purposefully maintained at high values, which can also be confirmed by the value of the inductor current in Figure 9. Despite the high values, the output voltage with S_2 also exhibits a permanent steady-state error, whereas there is no error with the proposed one.

In addition to a comparison with other SMC methods published in the literature, the proposed control mechanism is also tested under variations of the input voltage, load resistance and reference voltage in order to more thoroughly analyze and validate its efficacy.

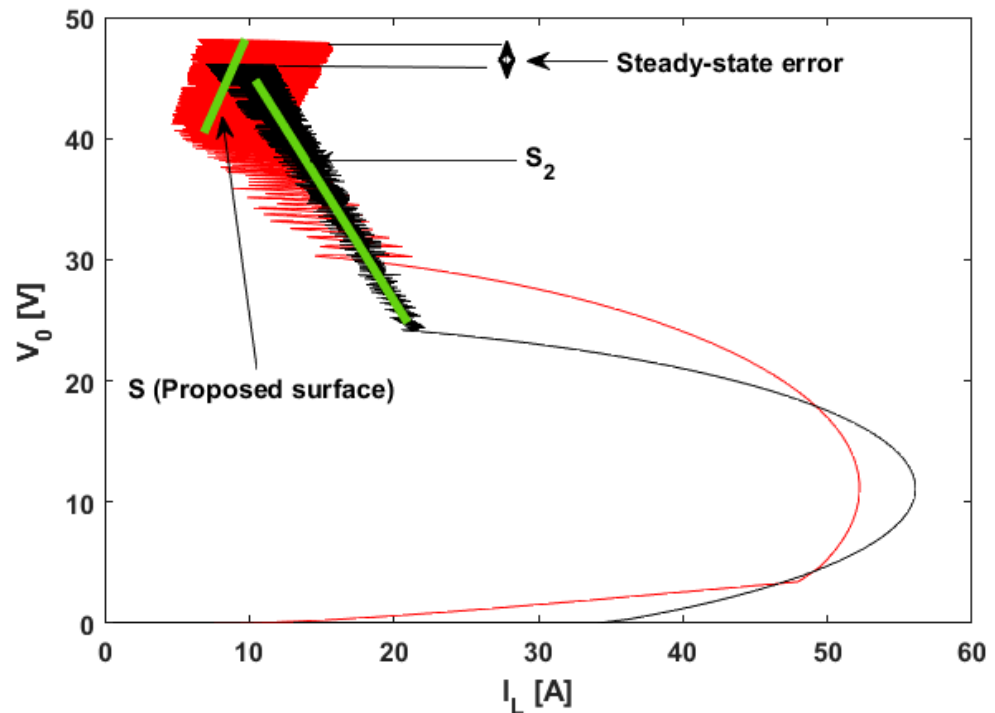


Figure 9. The motion of state variables on the proposed surface and S_2 .

Test-1: First, the DC input voltage E is changed from 12 to 25 V at the time $t = 0.045$ s and back again at the time $t = 0.12$ s, resulting in a 108% step variation. Figure 10 exemplifies the outcomes of the recommended technique. During an increase in E , an approximately 10% overshoot is produced. With the proposed procedure, the output voltage recovered to its previous value in 25 ms. In a similar fashion, the disruptive effect that occurred at $t = 0.12$ s and caused an 11.5% undershoot was also eliminated in about 25 ms by the proposed approach. On the other hand, (11) demonstrates that the source voltage (E) is an element that influences the switching frequency. Let us investigate the switching frequency in a closed loop and open loop under start-up and steady-state conditions before considering the impact of E . With (11), f_s can be easily calculated by recalling the control parameters in (2) and converter specifications in Table 2. The Δ value for the switching frequency is set to $\Delta = 22$, and the frequency is calculated as $f_s = 100$ kHz. During the start-up, it is obvious from Figure 11 that the interval type-2 fuzzy logic controlled f_s converges to the reference value of 100 kHz in a shorter amount of time in the case when f_s is not controlled. Furthermore, it should be emphasized that f_s is multi-oscillating and moves away from the reference orbit in an open loop.

Test-2: Under the 50% step load test, the effectiveness of the offered control techniques is also examined. During the simulation, the load resistance R is suddenly decreased from the nominal value of 20Ω to 10Ω at time $t = 0.045$ s and then back again at time $t = 0.12$ s. Figure 12 illustrates the dynamic reactions of the output voltage and output current to a rapid change in load resistance when $V_{ref} = 48$ V. Accordingly, during the step transition,

the output current smoothly increases, and then it returns to its initial value once the step transition happens again. These modifications result in the output voltage undershoot and overshoot of roughly 10.5% at $t = 0.045$ s and $t = 0.12$ s, respectively. The recommended SMC approach absorbs voltage variations in both cases within 18 ms. As can be observed from (11), load resistance also has an effect on the switching frequency, similarly to input voltage. This effect is plotted in Figure 13. The switching frequency varies significantly in the open loop during the load variations that take place during the times depicted in the linked graph and deviates greatly from the reference value. In contrast to the open loop, the same figure illustrates how T2FS exhibits a highly robust dynamic response to load variation at $t = 0.045$ s. The disturbance that takes place at $t = 0.12$ s has slightly affected the switching frequency, but the proposed IT2FS dampened this variation in approximately 50 ms.

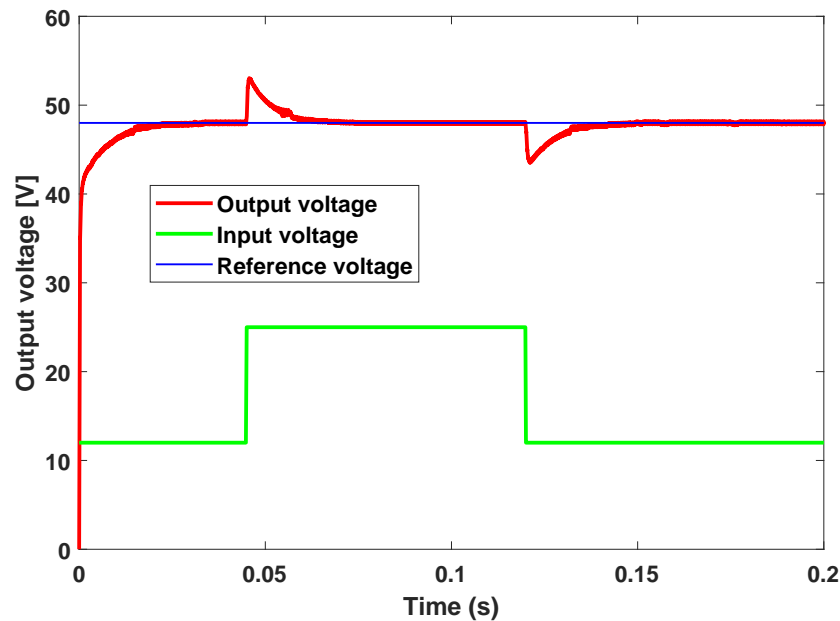


Figure 10. The dynamic response of SMC in the output voltage under an input voltage step change.

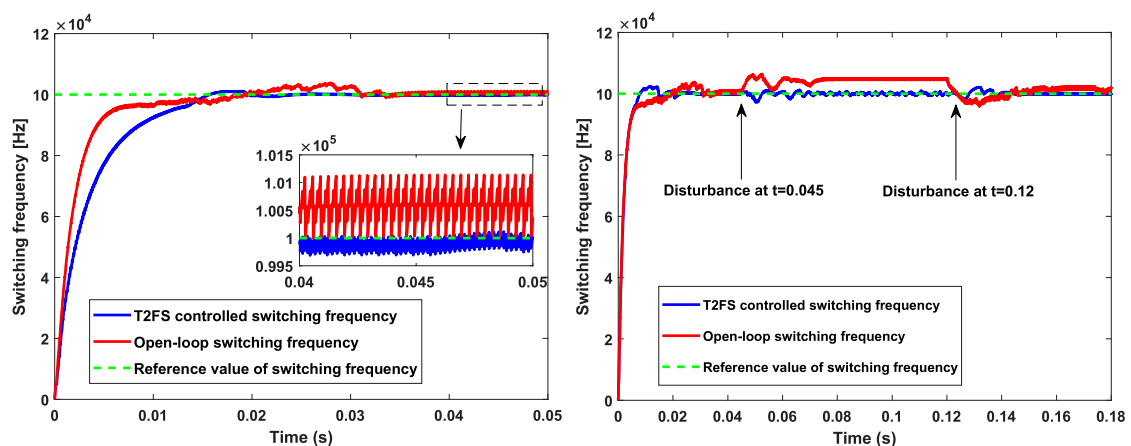


Figure 11. Open-loop and closed-loop control of switching frequency under start-up and input voltage disturbance.

Test-3: In the final test, the performances of both proposed control schemes are evaluated in response to changes in the reference value of the output voltage. The outcomes of the dynamic responses are shown in Figure 14. First, the reference voltage is decreased from 48 to 40 V at time $t = 0.045$ s and then back again at time $t = 0.12$ s. With a satisfactory dynamic response, the SMC tracks the changes in the reference trajectory at $t = 0.045$ and

$t = 0.12$. Additionally, the results show that the proposed approach can regulate the output voltage in a steady state both before and after the step changes. As for f_s , its behavior under this test is shown in Figure 15. The switching frequency exhibits a significant fluctuating behavior when left uncontrolled. Furthermore, in this case, it is much more oscillating compared to its controlled state. On the other hand, as can be seen from the same figure, the proposed IT2FS adequately maintains the switching frequency on the reference orbit in the steady state. Furthermore, the undershoot- and overshoot-caused reference voltage value has been eliminated in the proposed IT2FS.

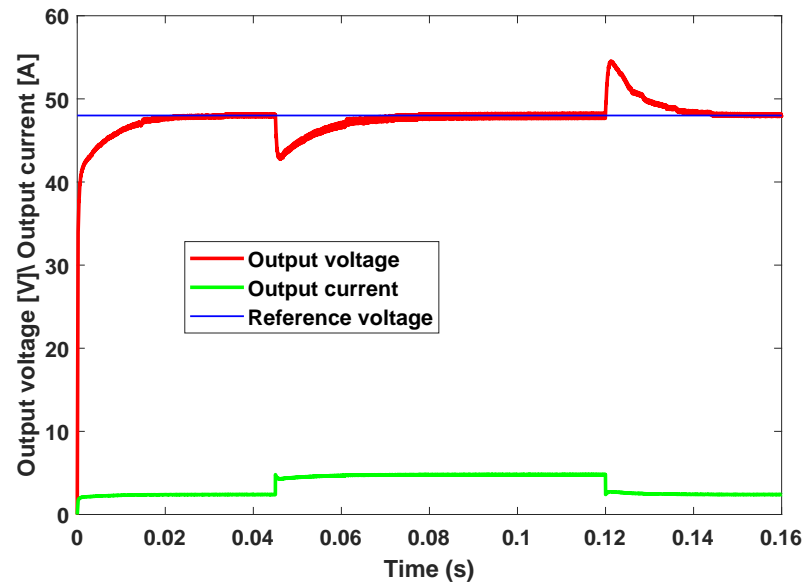


Figure 12. Transient response of recommended SMC in output voltage under load resistance step changes.

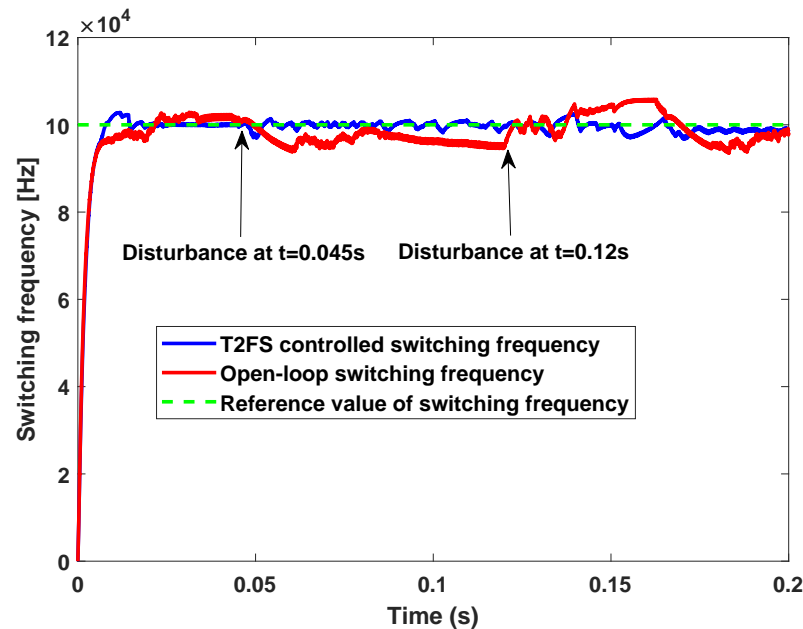


Figure 13. Transient response of switching frequency under load resistance step changes.

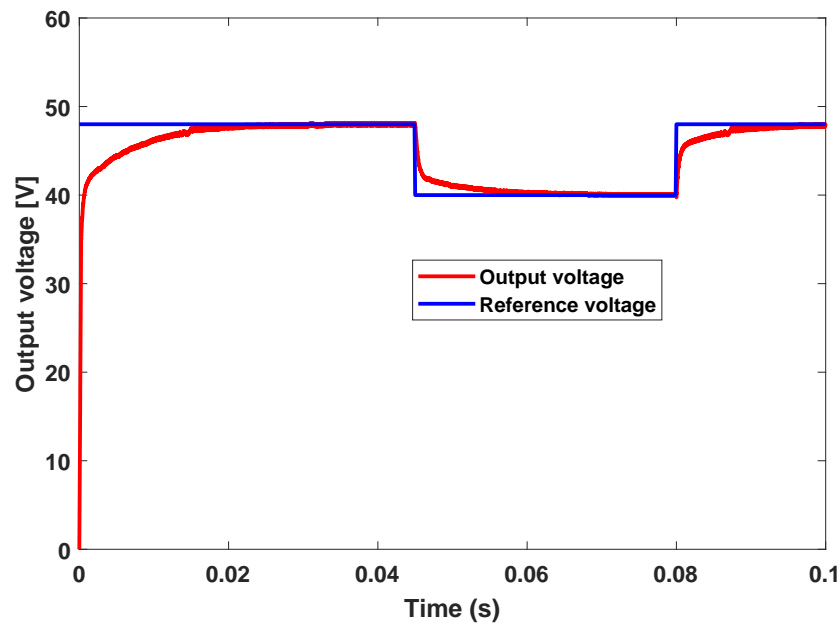


Figure 14. Dynamic response of SMC strategy in output voltage under reference voltage variations.

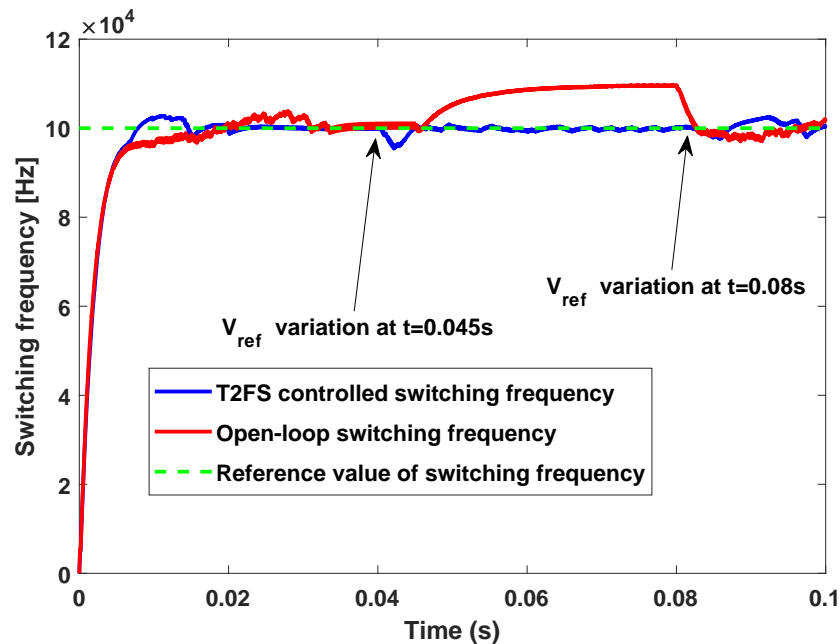


Figure 15. Dynamic response of switching frequency under reference voltage variations.

5.3. Comparison of the Proposed IT2FS with Another Constant-Switching Frequency Technique

In this study, two different methods, SMC and IT2FS, were presented. We compared the proposed sliding surface to various other surfaces in the literature and demonstrated its reliability. Similarly, to demonstrate the robustness of the IT2FS, this subsection compares it to the flip-flop approach described in the literature for obtaining a constant switching frequency. Reference [26] obtained a constant f_s by taking into account the components that cause the hysteresis band to vary. As shown in Figure 16, the approach presented in [26] has been constructed for this study. It is obvious that the load resistance value is also required for an adaptive band in this methodology. However, it is not feasible to measure the load resistance directly in practical applications. Hence, this technique is unsuitable for boost converters. Additionally, this strategy calls for the employment of more sensors due to its reliance on several inputs. On the other hand, the proposed IT2FS is unaffected by any of the issues stated above.

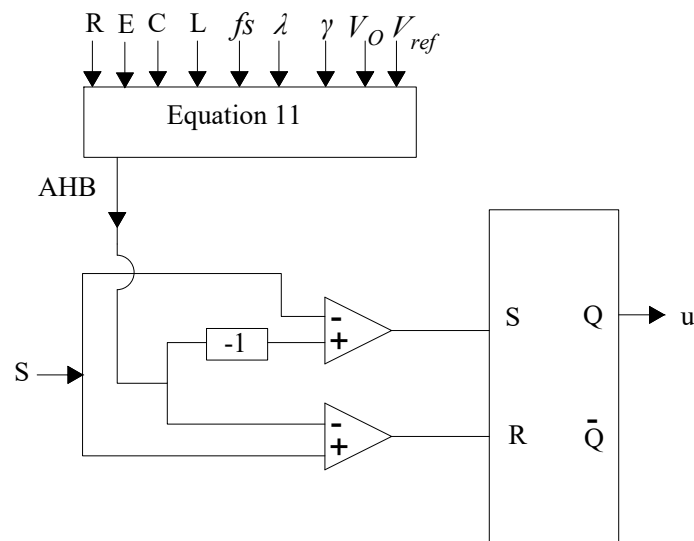


Figure 16. Adaptive hysteresis band with flip-flop.

5.4. Comparison with Existing Studies

The proposed SMC and IT2FS have been compared with four new studies concentrating on HM-SMC in Table 3 for additional validation of this study. The table makes it clear that the proposed control algorithm, which uses SMC for the output voltage/inductor current regulation and IT2SFS for switching frequency control, offers a fixed switching frequency and does not call for a switching frequency stability analysis. Table 4 was created to contrast this study with studies using other control methods, including the model predictive control, backstepping control, and fuzzy logic control. The study with the model predictive control is similar to this paper in that the switching signal is generated without the use of a modulator. However, the switching frequency in [27] is variable, and the use of a large number of sensors complicates the installation phase. Both references [28,29] use more sensors than this study and require a modulator. The phase of generating the switching signal with the modulator is more complicated than with the HM. Based on these comparisons, the approaches proposed in this study are simple in terms of experimental feasibility.

Table 3. Comparison of HM-SMC studies with proposed control methods from different perspectives.

| Ref | [1] | [19] | [30] | [31] | This Paper |
|------------------------------|----------|---------------|-------------------|---------------|------------|
| Converter type | Boost | Buck-Boost | Flyback | Sepic | Boost |
| Control approach | HM-SMC | HM-SMC | HM-SMC | HM-SMC | HM-SMC |
| Number of coefficients of S | 3 | 2 | 1 | 1 | 3 |
| Switching frequency | Constant | Variable | Slightly Constant | Variable | Constant |
| Control type for f_s | SMC | Not Available | Flip-flop | Not Available | IT2FS |
| Stability analysis for f_s | Require | Not Covered | Not Needed | Not Covered | Not Needed |

Table 4. Comparison of various control techniques with proposed control methods.

| Ref | [27] | [28] | [29] | This Paper |
|------------------------------|------------------|--------------|-------------|------------|
| Converter type | Boost | Boost | Buck-Boost | Boost |
| Control approach | Model predictive | Backstepping | Fuzzy logic | HM-SMC |
| Switching frequency | Variable | Constant | Constant | Constant |
| Number of sensors | 4 | 3 | 3 | 2 |
| Comparator usage | No | Yes | Yes | No |
| Simplicity in implementation | Complicated | Complicated | Complicated | Simple |

6. Conclusions and Future Works

In this study, HM-SMC was used to control the output voltage and inductor current of the DC–DC boost converter. Additionally, the IT2FS approach was used for the first time in this research to manage the switching frequency, which is intrinsically variable in HM-SMC. Through the integration of IT2FS into SMC in MATLAB/Simulink, the effectiveness of both controllers was assessed under various scenarios such as load resistance, reference of output voltage, and input voltage. The outcomes showed that both SMC and IT2FS are fairly successful in achieving good output voltage and switching frequency responses under the system disturbances.

The IT2FS faces a threat that will shrink its useable space despite offering extremely strong performance. Since IT2FS requires a digital signal processing memory for its operation, it is not applicable in analog circuits. The difficulty of the design process and the absence of a systematic design process of the IT2FS can be considered limitations of the proposed method. The experience of the designer has great importance in the design step.

In the future, T1FS and T2FS will be extended to a grid-connected LCL-filtered voltage source inverter with a double-band hysteresis scheme.

Author Contributions: Conceptualization, A.N. and N.A.; Methodology, N.A.; Software, G.B.; Validation, N.A.; Formal analysis, G.B.; Investigation, G.B.; Writing—original draft, N.A. and G.B.; Writing—review & editing, A.N.; Project administration, A.N. All authors have read and agreed to the published version of the manuscript.

Funding: This research received no external funding.

Institutional Review Board Statement: Not applicable.

Informed Consent Statement: Not applicable.

Data Availability Statement: Not applicable.

Conflicts of Interest: The authors declare no conflict of interest.

References

1. Repecho, V.; Biel, D.; Olm, J.M.; Fossas, E. Robust sliding mode control of a DC/DC Boost converter with switching frequency regulation. *J. Frankl. Inst.* **2018**, *355*, 5367–5383. [\[CrossRef\]](#)
2. Nandankar, P.V.; Bedekar, P.P.; Dhawas, P.K.V. Variable switching frequency control for efficient DC-DC converter. *Mater. Today Proc.* **2022**, *51*, 515–521. [\[CrossRef\]](#)
3. Pichan, M.; Arab Markadeh, G.; Blaabjerg, F. Continuous finite-time control of four-leg inverter through fast terminal sliding mode control. *Int. Trans. Electr. Energy Syst.* **2020**, *30*, e12355. [\[CrossRef\]](#)
4. Repecho, V.; Biel, D.; Olm, J.M.; Colet, E.F. Switching frequency regulation in sliding mode control by a hysteresis band controller. *IEEE Trans. Power Electron.* **2016**, *32*, 1557–1569. [\[CrossRef\]](#)
5. Repecho, V.; Biel, D.; Olm, J.M. A Simple Switching-Frequency-Regulated Sliding-Mode Controller for a VSI with a Full Digital Implementation. *IEEE J. Emerg. Sel. Top. Power Electron.* **2020**, *9*, 569–579. [\[CrossRef\]](#)
6. Komurcugil, H. Sliding mode control strategy with maximized existence region for DC–DC buck converters. *Int. Trans. Electr. Energy Syst.* **2021**, *31*, e12764. [\[CrossRef\]](#)
7. Komurcugil, H. Non-singular terminal sliding-mode control of DC–DC buck converters. *Control Eng. Pract.* **2013**, *21*, 321–332. [\[CrossRef\]](#)

8. Yazici, İ.; Yaylaci, E.K. Fast and robust voltage control of DC–DC boost converter by using fast terminal sliding mode controller. *IET Power Electron.* **2016**, *9*, 120–125. [[CrossRef](#)]
9. Komurcugil, H. Fast terminal sliding mode control for single-phase UPS inverters. In Proceedings of the 2011 IEEE International Symposium on Industrial Electronics, Gdansk, Poland, 27–30 June 2011; pp. 277–282.
10. Sen, D.; Saha, T.K.; Dey, J. Sliding mode control of double input buck buck–boost fused converter. *Asian J. Control* **2022**, *24*, 845–858. [[CrossRef](#)]
11. Chincholkar, S.H.; Jiang, W.; Chan, C.Y. A modified hysteresis-modulation-based sliding mode control for improved performance in hybrid DC–DC boost converter. *IEEE Trans. Circuits Syst. II Express Briefs* **2017**, *65*, 1683–1687. [[CrossRef](#)]
12. Chen, Z.; Chen, Y.; Yan, Z. Simplified hysteresis sliding-mode control for superbuck converter. *IEEE Trans. Circuits Syst. II Express Briefs* **2020**, *67*, 3212–3216. [[CrossRef](#)]
13. Chan, C.Y. Adaptive sliding-mode control of a novel buck-boost converter based on Zeta converter. *IEEE Trans. Circuits Syst. II Express Briefs* **2021**, *69*, 1307–1311. [[CrossRef](#)]
14. Ramos-Paja, C.A.; Montoya, D.G.; Bastidas-Rodríguez, J.D. Sliding-mode control of a CuK converter for voltage regulation of a dc-bus. *Sustain. Energy Technol. Assess.* **2020**, *42*, 100807. [[CrossRef](#)]
15. Balta, G.; Güler, N.; Altin, N. Modified Fast Terminal Sliding Mode Control for DC-DC Buck Power Converter with Switching Frequency Regulation. *Int. Trans. Electr. Energy Syst.* **2022**, *2022*, 5076611. [[CrossRef](#)]
16. Nizami, T.K.; Chakravarty, A. Neural network integrated adaptive backstepping control of DC-DC boost converter. *IFAC-PapersOnLine* **2020**, *53*, 549–554. [[CrossRef](#)]
17. Yang, T.; Liao, Y. Discrete Sliding Mode Control Strategy for Start-Up and Steady-State of Boost Converter. *Energies* **2019**, *12*, 2990. [[CrossRef](#)]
18. Guldemir, H. Sliding mode control of DC-DC boost converter. *J. Appl. Sci.* **2005**, *5*, 588–592. [[CrossRef](#)]
19. Guldemir, H. Modeling and sliding mode control of dc-dc buck-boost converter. In Proceedings of the 6th International Advanced Technological Symp, Elazığ, Turkey, 16–18 May 2011; Volume 4, pp. 475–480.
20. Goudarzian, A.; Khosravi, A.; Raeisi, H.A. Optimized sliding mode current controller for power converters with non-minimum phase nature. *J. Frankl. Inst.* **2019**, *356*, 8569–8594. [[CrossRef](#)]
21. Canciello, G.; Cavallo, A.; Schiavo, A.L.; Russo, A. Multi-objective adaptive sliding manifold control for More Electric Aircraft. *ISA Trans.* **2020**, *107*, 316–328. [[CrossRef](#)]
22. Cavallo, A.; Canciello, G.; Russo, A. Buck-boost converter control for constant power loads in aeronautical applications. In Proceedings of the 2018 IEEE Conference on Decision and Control (CDC), Miami, FL, USA, 17–19 December 2018; pp. 6741–6747.
23. Sharifian, A.; Sasansara, S.F.; Ghadi, M.J.; Ghavidel, S.; Li, L.; Zhang, J. Dynamic performance improvement of an ultra-lift Luo DC–DC converter by using a type-2 fuzzy neural controller. *Comput. Electr. Eng.* **2018**, *69*, 171–182. [[CrossRef](#)]
24. Hemeyine, A.V.; Abbou, A.; Bakouri, A.; Mokhlis, M.; El Moustapha, S.M.O.M. A robust interval Type-2 fuzzy logic controller for variable speed wind turbines based on a doubly fed induction generator. *Inventions* **2021**, *6*, 21. [[CrossRef](#)]
25. Bennaoui, A.; Saadi, S. Type-2 fuzzy logic PID controller and different uncertainties design for boost DC–DC converters. *Electr. Eng.* **2017**, *99*, 203–211. [[CrossRef](#)]
26. Ortiz-Castrillón, J.R.; Mejía-Ruiz, G.E.; Muñoz-Galeano, N.; López-Lezama, J.M.; Cano-Quintero, J.B. A sliding surface for controlling a semi-bridgeless boost converter with power factor correction and adaptive hysteresis band. *Appl. Sci.* **2021**, *11*, 1873. [[CrossRef](#)]
27. Irmak, E.; Güler, N. A model predictive control-based hybrid MPPT method for boost converters. *Int. J. Electron.* **2020**, *107*, 1–16. [[CrossRef](#)]
28. Deo, R.N.; Shrivastava, A.; Chatterjee, K. Implementation of sliding mode backstepping controller for boost converter in real-time for LED application. *Expert Syst.* **2022**, e13095. [[CrossRef](#)]
29. Şahin, M.E.; Okumuş, H.İ. Parallel-connected buck–boost converter with FLC for hybrid energy system. *Electr. Power Components Syst.* **2021**, *48*, 2117–2129. [[CrossRef](#)]
30. Ramos-Paja, C.A.; Montoya, O.D.; Grisales-Noreña, L.F. Adaptive Sliding-Mode Controller for Flyback-Based PV Systems Featuring Constant Switching Frequency. *Mathematics* **2022**, *10*, 1255. [[CrossRef](#)]
31. Goudarzian, A.; Khosravi, A.; Raeisi, H.A. A new approach in design of sliding-mode voltage-controller for a SEPIC. *Int. J. Dyn. Control* **2021**, *9*, 1197–1209. [[CrossRef](#)]

Disclaimer/Publisher’s Note: The statements, opinions and data contained in all publications are solely those of the individual author(s) and contributor(s) and not of MDPI and/or the editor(s). MDPI and/or the editor(s) disclaim responsibility for any injury to people or property resulting from any ideas, methods, instructions or products referred to in the content.